

Accepted Manuscript

Title: Simulation of solid-state magnetocaloric refrigeration systems with Peltier elements as thermal diodes

Author: Behzad Monfared

PII: S0140-7007(16)30373-5

DOI: <http://dx.doi.org/doi: 10.1016/j.ijrefrig.2016.11.007>

Reference: IJIR 3475

To appear in: *International Journal of Refrigeration*

Received date: 17-8-2016

Revised date: 8-11-2016

Accepted date: 13-11-2016

Please cite this article as: Behzad Monfared, Simulation of solid-state magnetocaloric refrigeration systems with Peltier elements as thermal diodes, *International Journal of Refrigeration* (2016), <http://dx.doi.org/doi: 10.1016/j.ijrefrig.2016.11.007>.

This is a PDF file of an unedited manuscript that has been accepted for publication. As a service to our customers we are providing this early version of the manuscript. The manuscript will undergo copyediting, typesetting, and review of the resulting proof before it is published in its final form. Please note that during the production process errors may be discovered which could affect the content, and all legal disclaimers that apply to the journal pertain.



Simulation of solid-state magnetocaloric refrigeration systems with Peltier elements as thermal diodes

Behzad Monfared^{a,*}

^a KTH Royal Institute of Technology, School of Industrial Engineering and Management, Department of Energy Technology, Brinellvägen 68, SE-100 44 Stockholm, Sweden

* Corresponding author. Tel.: +46 8 790 81 54; fax.: +46 8 20 41 61.

E-mail address: behzadam@kth.se (Behzad Monfared)

Accepted Manuscript

Highlights

- Magnetic refrigeration system with Peltier elements as thermal diodes is modeled
- The physical and numerical models are explained in great detail
- The model is verified and used for a parametric study
- The effect of key parameters in the performance of the system is discussed

Abstract

Magnetic refrigeration as an alternative for vapor-compression technology has been the subject of many recent studies. Most of the studies focus on systems with limited cycle frequency in which a fluid transfers heat to and from the magnetocaloric material. A suggested solution for increasing the frequency is use of solid-state magnetic refrigeration in which thermal diodes guide the heat from the cold end to the warm end. In this work a solid-state refrigeration system with Peltier elements as thermal diodes is modeled in details unprecedented. The performance of Peltier elements and magnetocaloric materials under their transient working conditions after reaching cyclic steady state are simulated by two separate computer models using finite element method and finite volume method. The models, in parts and as a whole, are verified. The verified finite element model is used for a parametric study and the results are analyzed.

Keywords: magnetic refrigeration, solid-state, Peltier element, thermal diode, heat gate, hybrid.

Nomenclature

Symbols

a	lower integral limit [m]
A	cross section area [m ²]
b	higher integral limit [m]
B	magnetic field [T]
$\{BC\}$	boundary conditions vector [W]
c	points where Peltier effect occur [m]
$[C]$	heat capacity matrix [JK ⁻¹]
c_p	heat capacity [Jkg ⁻¹ K ⁻¹]
dx	differential element [m]
El_{PE}	electric consumption of Peltier elements [W]
eq	equivalent

erf	error function
$\{fl\}$	heat generation vector [W]
i	index of cell in discretized equations
I	electric current activating Peltier element [A]
j	index of time step
k	thermal conductivity [$\text{Wm}^{-1}\text{K}^{-1}$]
$[K]$	stiffness matrix (diffusion) [WK^{-1}]
L	length [m]
$[MCE]$	magnetocaloric effect matrix [WK^{-1}]
$[PE]$	Peltier effect matrix [WK^{-1}]
$prev.$	previous time step
$\{Q\}$	heat generation vector [W]
Q_C	cooling capacity [W]
Q_{cond}	conduction heat transfer rate [W]
Q_H	heating capacity [W]
R	share of adjacent cells from Peltier effect
s	entropy [$\text{Jkg}^{-1}\text{K}^{-1}$]
t	time [s]
T	temperature [K]
$\{T\}$	temperature vector [K]
T_0	initial temperature (Equation 12 and Equation 13) [K]
T_1	temperature at boundary (Equation 12 and Equation 13) [K]
T_{CE}	temperature at the cold end, Dirichlet boundary condition [K]
T_{HE}	temperature at the warm end, Dirichlet boundary condition [K]
W_{mag}	rate of magnetic work [W]

x	distance from origin [m]
α	Seebeck coefficient [VK^{-1}]
αIT	Peltier effect [W]
δ	Dirac delta function [m^{-1}]
Δt	length of time step [s]
Δx	length of cell [m]
η_c	Carnot efficiency, ratio of the actual COP to that of a Carnot cycle [%]
ρ	density [kgm^{-3}]
σ	electrical conductivity [Sm^{-1}]
$\tau_1, \tau_2, \tau_3, \tau_4$	duration of the cycle processes (described in section 2.1) [s]
ψ	arbitrary test function (FEM)

Abbreviations

C	ceramic
COP	coefficient of performance
Cu	copper
MCM	magnetocaloric material
PE	Peltier element
SC	semi-conductor

1 Introduction

In recent years, a lot of research work has been done on magnetic refrigeration at room temperature as the most promising alternative to vapor-compression technology (Qian et al. 2016). Magnetocaloric materials (MCM) are used as the refrigerant in magnetic refrigeration. When the magnetocaloric materials are magnetized they become warm. While the magnetocaloric materials are kept magnetized, the heat can be removed from them; thus, when the materials are demagnetized afterwards, they become relatively cold and ready to accept heat from the heat source. Although the magnetocaloric effect is only a few Kelvin, larger temperature spans are usually created via regeneration by pumping a heat transfer fluid back and forth through porous magnetocaloric materials after each magnetization or demagnetization process; that is, the

magnetocaloric materials serve as both refrigerant and regenerator. Two main drawbacks of such a design are: high pressure drop in the porous media, which leads to large viscous dissipation and pumping power consumption, and limited frequency of the cycle, which results in low cooling capacity. Solid-state magnetic refrigeration, in which heat is transferred via conduction or via active components instead of advection, is proposed to overcome these drawbacks (Kitanovski et al. 2015). Furthermore, in a solid-state magnetic refrigeration device, the complexity of the fluid circuit and the extra losses due to friction in its moving parts (such as valves, seals, and pump) are avoided.

In a solid-state magnetic refrigeration device, the axial heat transfer is controlled to limit the unfavorable heat transfer from the warm end to the cold end. Different solutions for hindering axial heat transfer in one direction and enhancing it in the opposite direction (thermal diodes) are covered by Kitanovski et al. (2015) among which Peltier elements are the most accessible ones at the time being as commercially available products. Considering that the Peltier elements consume power to pump heat in the desired direction, such a combination of magnetocaloric materials and Peltier elements can also be viewed as a hybrid refrigeration system.

Tasaki et al. (2012) have compared the performance of a magnetic refrigeration system with heat transfer fluid with that of a solid-state one for mobile air-conditioning application. For that purpose, a solid-state magnetic refrigeration unit composed of layers of magnetocaloric materials sandwiched between thermal diodes is modeled. In their model, the magnetocaloric material has a constant 5 K adiabatic temperature change and constant heat capacity with no temperature gradient along the axial direction, implying infinite thermal conductivity. The thermal diodes used in the model have infinite thermal conductivity when they are active and zero thermal conductivity at other times.

Tomc et al. (2013, 2014) have modeled a long, thin sheet of magnetocaloric material with 40 Peltier elements on each side. When the magnetocaloric material is magnetized, Peltier elements on one side of it pump the heat from magnetocaloric material to the warm heat exchanger. In the warm heat exchanger a fluid flows along the axial direction of the magnetocaloric sheet from the cold end to the warm end. When the magnetocaloric material is demagnetized, the rest of the Peltier elements, which served as insulation in the previous processes, pump the heat from the cold heat exchanger to the magnetocaloric material. In the cold heat exchanger a fluid flows along the axial direction from the warm end to the cold end. The simplifications made in this study are that a constant temperature span of 0.3 K is assumed at the two ends of the Peltier elements, steady state performance of Peltier elements are used to estimate their performance during the cycle, and the longitudinal thermal conduction through the magnetocaloric material is neglected.

Olsen et al. (2014) have investigated the limits for a solid-state magnetic refrigeration device to be used in mobile air-conditioning units. The design of the device modeled by them is similar to what is modeled by Tasaki et al. (2012). No particular mechanism is considered for the thermal

diodes, but it is assumed that their thermal conductivity changes from zero (inactive diodes preventing heat transfer in adverse direction) to a finite value (active diodes allowing heat transfer in the desired direction).

Silva et al. (2014) have modeled a number of magnetocaloric material layers sandwiched between thermal diodes in a stack, similar to the design used by Tasaki et al. (2012) and Olsen et al. (2014). It is assumed that the thermal conductivity of the diodes changes from zero to a finite value when excited by a magnetic field with negligible work for excitation.

Monfared (2016) has investigated the limit to the gain in cooling capacity from increased frequency of a design similar to the one presented by Tasaki et al. (2012) and Olsen et al. (2014) using non-ideal magnetocaloric materials with limited conductivity and two different mechanisms as non-ideal thermal diodes with conductivities limited by the materials used in them.

Bartholomé et al. (2016) have investigated replacing the compressor of a vapor-compression cycle with magnetocaloric materials, a magnet assembly, and thermal diodes. Their work is different from what is usually considered as magnetic refrigeration in the sense that the gaseous refrigerant is still present and the refrigerant becomes cold through an expansion process, not through demagnetization. Li et al. (2016) have investigated the use of thermal diodes together with materials showing high electrocaloric effect.

A reason why in some of the above mentioned works hypothetical thermal diodes are considered is that such passive thermal diodes are not readily available. A commercially available thermal diode, but less attractive in terms of power consumption as it is an active device, is the Peltier element, which is used in this work. An advantage of Peltier elements over passive thermal diodes is that the rate of heat transfer through them can be adjusted by controlling the electric current to match the demand during their varying working conditions. In this work, the transient behavior of the Peltier elements are accurately modeled. This is necessary since during magnetic refrigeration cycles, especially with high frequency, which is a motivation behind developing solid-state magnetic refrigeration devices, the Peltier elements work at conditions far from steady state. The modeling is done with two approaches: finite element method (FEM) and finite volume method (FVM) and validated at different stages. In addition, the FEM model is used in a parametric study, the results of which are discussed at the end.

2 Modeling

2.1 The physical model

The working principle of the magnetic refrigeration device modeled in this study is shown schematically in Fig. 1. The cycle consists of four processes: a) the odd magnetocaloric material layers, shown by red in Fig. 1a, are magnetized and therefore have become a few Kelvin warmer. There is no current in the Peltier elements and they are practically passive pieces of material with

rather low conductivity. b) Every other (even) Peltier element is active and pumps heat from the warm (odd) magnetocaloric material layers to colder (even) ones. c) All Peltier elements are inactive and the other pieces of magnetocaloric material (even layers) are magnetized and warm, but the previously magnetized materials (odd layers) are now cold because of demagnetization. d) The (odd) Peltier elements which were inactive so far are active now and pump heat from the warm magnetocaloric material layers to the colder ones. After the fourth process the second cycle similar to the first one starts. The change in the field is modeled as ramp and the electric current change is modeled as step function.

The Peltier elements consist of two semiconductor legs connected by a layer of copper, which is electrically insulated by a layer of ceramic (Fig. 2). Due to Peltier effect, when a Peltier element is excited by an electrical current, heat is removed from the Cu-SC junction at the cold end and released in the Cu-SC junction at the hot end of each leg of the Peltier element with the rate of αIT as a surface effect. Some of the consumed electric power turns into heat due to Joule heating. Another major loss mechanism in Peltier elements is the axial conduction from the warm end to the cold end. Further details about the Peltier elements are covered by Goldsmid (1964). Since the cooling power of a single Peltier element is usually not enough, a number of them can be put together to form thermoelectric modules (Fig. 3) (Hodes 2005).

Assuming that the properties of the two legs are similar, it is of convenience to model only one leg and the corresponding cross section areas of Cu, C, and MCM. Then, the total cooling or consumed electric power is calculated by multiplying the energy rates by two for a single Peltier element and by the number of Peltier elements for a thermoelectric module. As can be inferred from Fig. 2, the cross section of a semiconductor leg is different from the corresponding cross section areas of Cu, C, and MCM. The sequence of placement of the materials is shown schematically in Fig. 4 for a case with three layers of magnetocaloric materials. However, the number of layers of magnetocaloric material can be less or more.

The MCM is modeled using the measured data presented by Lozano et al. (2014) for gadolinium. However, for layering, its Curie temperature is modified to match the working temperatures as explained by Monfared and Palm (2015). In the simulations, the Curie temperature of each layer of MCM is chosen as the average temperature of that layer during a cycle after reaching cyclic steady state. For the MCM geometry used in this study, which is a thin prism parallel to the field lines, the demagnetizing factor is small, as modeled in COMSOL, and results in about 5-7% difference between the external and internal field. This difference is neglected in the study as it does not influence the conclusions.

When the magnetic field varies, an electromotive force is induced in the electric conductor, the magnetocaloric material in this study, which senses the field. The eddy currents caused by the induced electromotive force result in Joule heating. In this study, the heat produced by eddy currents, as modeled in COMSOL, is few orders of magnitude smaller than the cooling capacities calculated by the models explained in section 2.3; therefore, the eddy current losses are not

included in the study. The low eddy current losses are to be expected considering the rather low electrical conductivity of gadolinium (one-third of electrical steel), which limits the current driven by the induced electromotive force; the short distance over which the current can flow because of the small dimensions of the magnetocaloric material layers; the rather low or moderate frequencies used in the study.

The properties of the materials are constant in simulations except for the rate of entropy change per unit magnetic field change and the heat capacity of MCM which are functions of both temperature and magnetic field. The Thomson effect in Peltier elements, which is of secondary importance, is zero when the properties are constant (Goldsmid 1964).

2.2 Mathematical model

By using an energy balance over an arbitrarily small element of a Peltier element (Fig. 5), Equation 1 is derived. Since the Peltier effect is not a bulk effect, it is not shown in Fig. 5.

$$\frac{\partial}{\partial x} \left(kA \frac{\partial T}{\partial x} \right) + \frac{I^2}{\sigma A} \pm \delta(x - c) \alpha IT = \rho A c_p \frac{\partial T}{\partial t} \quad \text{Equation 1}$$

The terms in Equation 1 from left to right represent thermal conduction (diffusion), Joule heating caused by the electric current in active Peltier elements, Peltier effect, and heat storage. The Peltier effect appears only at the SC-Cu junction as a surface phenomenon, so in the 1D model it is shown by Dirac delta function at points $x=c$, where c represents coordinates for SC-Cu junctions. In the Peltier effect term, negative and positive signs are for the heating end and the cooling end of Peltier elements.

The energy balance equation over MCM elements (Equation 2) is adapted from (Engelbrecht 2008). The original equation is verified and used extensively in magnetic refrigeration literature.

$$\frac{\partial}{\partial x} \left(kA \frac{\partial T}{\partial x} \right) - \rho AT \frac{\partial s}{\partial B} \frac{\partial B}{\partial t} = \rho A c_p \frac{\partial T}{\partial t} \quad \text{Equation 2}$$

To facilitate computation, one equation (Equation 3) can be written for the whole array of Peltier elements (including their copper and ceramic layers) and the magnetocaloric materials. This can be achieved by defining I and $\partial s/\partial B$ as functions of both space and time with zero values for MCM and PE, respectively.

$$\frac{\partial}{\partial x} \left(kA \frac{\partial T}{\partial x} \right) + \frac{I^2}{\sigma A} - \rho AT \frac{\partial s}{\partial B} \frac{\partial B}{\partial t} \pm \delta(x - c) \alpha IT = \rho A c_p \frac{\partial T}{\partial t} \quad \text{Equation 3}$$

The properties and also the cross section area are defined as space functions acquiring the values related to the element for which Equation 3 is being applied.

The coefficient of performance, COP, is defined in Equation 4 as the ratio of cooling capacity to the power input to the system.

$$\text{COP} = \frac{Q_C}{Q_H - Q_C} \quad \text{Equation 4}$$

2.3 Numerical models

Two different numerical approaches are used in this work. For two reasons finite element method (FEM) seems more straightforward compared to finite volume method (FVM): first, the Peltier effect happens at a point in a 1D model, as a surface phenomenon, not along an element as a bulk effect; therefore, it is not immediately obvious how the effect should be divided between two finite volumes when it happens at their border or how it can be modeled as a surface effect when it happens within a finite volume. Second, taking variations of conductivity and cross section area between two nodes into account needs extra work in FVM. However, in this work, in addition to developing a FEM numerical model, a FVM numerical model is also developed in which these two difficulties are addressed.

Since in the numerical models the temperature dependent properties are unknown before acquiring the solution for each time step, the guess values, which are the temperatures at the same time step in the previous cycle, can be updated through iteration until the change in the temperatures in two consecutive iterations becomes smaller than a tolerance, $0.1\mu\text{K}$ in this study.

2.3.1 FEM

The array of Peltier elements and MCM is divided into a number of elements, which can have different lengths, and temperature nodes are defined at the border of the elements.

For an arbitrary test function $\psi(x)$ which is differentiable once and is zero at inner boundaries, the weak form of Equation 3 can be derived (Equation 5). In this equation, a and b indicate the lower and higher limits of integration, which can be performed over the whole length of the PE-MCM array or only one element:

$$\int_a^b \psi(x) \frac{\partial}{\partial x} \left(kA \frac{\partial T}{\partial x} \right) dx + \int_a^b \psi(x) \frac{I^2}{\sigma A} dx - \int_a^b \psi(x) \rho AT \frac{\partial s}{\partial B} \frac{\partial B}{\partial t} dx \pm \int_a^b \psi(x) \delta(x - c) \alpha IT dx = \int_a^b \psi(x) \rho Ac_p \frac{\partial T}{\partial t} dx \quad \text{Equation 5}$$

After integration by part to reduce the order of the derivatives of the diffusion term, Equation 6 is derived, in which boundary conditions can be seen separately (the first term):

$$\left[\psi(x) kA \frac{\partial T}{\partial x} \right]_a^b - \int_a^b \frac{\partial \psi(x)}{\partial x} kA \frac{\partial T}{\partial x} dx + \int_a^b \psi(x) \frac{I^2}{\sigma A} dx - \int_a^b \psi(x) \rho AT \frac{\partial s}{\partial B} \frac{\partial B}{\partial t} dx \pm \int_a^b \psi(x) \delta(x - c) \alpha IT dx = \int_a^b \psi(x) \rho Ac_p \frac{\partial T}{\partial t} dx \quad \text{Equation 6}$$

Equation 7 is the discretized equation in matrix form after using Galerkin method and linear temperature gradient in each element (Dhatt et al. 2012).

$$(-[K] + [MCE] + [PE])\{T\} + \{Q\} + \{BC\} = [C] \left\{ \frac{\partial T}{\partial t} \right\} \quad \text{Equation 7}$$

In Equation 7, $[K]$ is diffusion matrix, $[MCE]$ is magnetocaloric effect matrix, $[PE]$ is Peltier effect matrix, $\{T\}$ is temperature vector, $\{Q\}$ is heat generation vector, and $[C]$ is heat capacity matrix. After discretizing the time partial derivative of temperature, Equation 8 can be written.

$$\left(\frac{[C]}{\Delta t} + [K] - [MCE] - [PE]\right)\{T\} = \frac{[C]}{\Delta t}\{T\}^{prev.} + \{Q\} + \{BC\} \quad \text{Equation 8}$$

2.3.2 FVM

The array of Peltier elements and MCM is divided into a number of cells with equal lengths, and the temperature nodes are defined at their centers (Fig. 6).

The array is made of different materials and adjacent cells can have different cross section areas and thermal conductivities. Since the temperature nodes are at the center of the cells, it is needed that kA be replaced by an equivalent value, $(kA)_{eq}$, in a way that $\frac{\partial}{\partial x}\left(kA \frac{\partial T}{\partial x}\right)$ is always calculated correctly even when the cross section area and the thermal conductivity of the materials between the two temperature nodes vary, as is the case between T_a and T_b in Fig. 7.

Energy balance over the common interface of the cells gives Equation 9 and Equation 10:

$$k_a A_a \frac{(T_{ab} - T_a)}{\Delta x/2} = k_b A_b \frac{(T_b - T_{ab})}{\Delta x/2} \quad \text{Equation 9}$$

$$(kA)_{eq,ab} \frac{(T_b - T_a)}{x\Delta} = k_a A_a \frac{(T_{ab} - T_a)}{\Delta x/2} \quad \text{Equation 10}$$

By eliminating the temperature at the interface, T_{ab} , between Equation 9 and Equation 10, Equation 11 is derived. The same result is obtained if instead of Equation 10 a similar equation is written for cell b.

$$(kA)_{eq,ab} = 2 \frac{k_a A_a k_b A_b}{k_a A_a + k_b A_b} \quad \text{Equation 11}$$

Another difficulty in using FVM is that the Peltier effect, as a surface effect, takes place at the interface of two adjacent copper and semiconductor cells; therefore, it needs to be divided between them. The analytical solution to the transient heat equation for a long bar with Dirichlet boundary condition, $T(0,t)=T_1$ and initial condition of $T=T_0$ is found by the aid of Laplace transform (Equation 12) (Crank 1975).

$$T(x,t) = T_1 - (T_1 - T_0) \operatorname{erf}\left(\frac{x}{2\sqrt{\alpha t}}\right) \quad \text{Equation 12}$$

Therefore, the heat transfer rate at $x=0$ is given by Equation 13.

$$-kA \frac{\partial T}{\partial x}\bigg|_{x=0} = (T_1 - T_0) \frac{A}{\sqrt{\pi t}} \sqrt{\rho k c_p} \quad \text{Equation 13}$$

Considering the copper and semiconductor parts of the Peltier elements as two bars, for which Equation 13 can be written, with common temperature at the interface, shares of the adjacent copper and semiconductor cells are approximated using Equation 14 and Equation 15.

$$R_{Cu} = \frac{A_{Cu}\sqrt{\rho_{Cu}k_{Cu}c_{p,Cu}}}{A_{Cu}\sqrt{\rho_{Cu}k_{Cu}c_{p,Cu}} + A_{SC}\sqrt{\rho_{SC}k_{SC}c_{p,SC}}} \quad \text{Equation 14}$$

$$R_{SC} = \frac{A_{SC}\sqrt{\rho_{SC}k_{SC}c_{p,SC}}}{A_{Cu}\sqrt{\rho_{Cu}k_{Cu}c_{p,Cu}} + A_{SC}\sqrt{\rho_{SC}k_{SC}c_{p,SC}}} \quad \text{Equation 15}$$

The discretized form of Equation 3 used in FVM is Equation 16.

$$\frac{k_{eq,i,i+1} \frac{T_{i+1}^j - T_i^j}{\Delta x} - k_{eq,i,i-1} \frac{T_i^j - T_{i-1}^j}{\Delta x}}{\Delta x} A_i \Delta x + \frac{I^2}{\sigma_{A_{pel}}} \Delta x - \rho_i A_i T_i^{j-1} \frac{\partial s}{\partial B} \frac{\partial B}{\partial t} \Delta x \pm RaIT_i^j = \rho_i A_i c_{p,i} \frac{T_i^j - T_i^{j-1}}{\Delta t} \Delta x \quad \text{Equation 16}$$

R is a ratio calculated using Equation 14 or Equation 15 depending on the cell for which the discretized equation is written.

3 Results and validation

To validate the model of Peltier elements, a simple case of one Peltier element and no MCM is compared to the built 3D model of “*Thermoelectric Leg*” (Application ID: 16365) from the application gallery developed by COMSOL¹. Table 1 and Fig. 8 show the results of the comparison. The differences in output values of the models in percentage are given in the last column of the table.

To validate the physical and numerical model of magnetocaloric effect, a bar with MCM in the middle part and insulating materials at two ends is modeled. For a transient condition in which the magnetic field increases linearly the temperature of the middle part reaches the adiabatic temperature change of MCM corresponding to the known values reported by Lozano et al. (2014). It shows that the magnetocaloric effect, heat storage, and conduction are modeled correctly.

The two FEM and FVM models are validated against each other, as well. Table 2 summarizes the input values for two different simulations by which FEM and FVM models are validated. The results of the tests have also been discussed in section 4.

¹ <https://www.comsol.se/model/thermoelectric-leg-16365>

Table 3 shows the results of the tests. Since a small area corresponding to one leg of a Peltier element is modeled, the energy rates calculated by the models are small. Therefore, the values per kg of MCM are also shown. The differences between the values calculated by the two models (FEM and FVM) and their average are listed in the last two columns of Table 3 as “error”. Fig. 9 shows the temperatures along the bed averaged during a cycle after reaching cyclic steady state for test 2. Video 1, (only available in the electronic version as Supplementary content) shows temperatures for the whole cycle.

Iteration to find the values of the temperature dependent parameters increases the computation time to reach steady state considerably. Nevertheless, it does not change the results when compared to the solution without iteration.

Now that the models are validated, the effect of varying two parameters, length of SC and electric current, are investigated for test 2 (Fig. 10). There are, as discussed in Section 4, numerous interrelated parameters affecting the performance. Thus, this is not a comprehensive parametric study, e.g. aiming at optimizing the performance, which is not within the scope of this article.

4 Discussion and conclusions

Two separate numerical models using FEM and FVM are developed to simulate the performance of a solid-state magnetic refrigeration device with Peltier elements as thermal diodes. The models simulate the transient performance of PE and MCM during a cycle. Comparison of the developed model for the Peltier element with a COMSOL model shows the validity of our physical and numerical model for Peltier elements. Through comparing the results, the finite volume model and the finite element model are validated against each other.

Two difficulties in modeling the array of MCM and PE using FVM, namely the occurrence of the Peltier effect at the boundaries of cells as a surface phenomenon and variation in kA values from node to node, are addressed. Close results obtained from the finite volume model and the finite element model indicate that the two problems are solved successfully.

The fact that evaluating temperature dependent properties through iteration at each time step did not change the results is not unexpected. What makes iteration unnecessary is that the guess values for temperature, which are the temperatures at previous cycle, are extremely close to the temperatures to be calculated when reaching the steady state, which is the state of interest in this study.

Unlike conventional magnetic refrigeration devices with heat transfer fluid, as can be seen in Fig. 9, the temperature gradient along each MCM layer has a negative slope, while the slope is positive for the array as a whole. This is the result of using thermal diodes (transferring heat to the left side and from the right side of each layer) and finite thermal conductivity of MCM.

The reduced COP value in test 2 compared to test 1 can be associated to two factors: Joule heating in the Peltier elements has become four times larger because of the twofold increase in the current; the maximum theoretical COP, Carnot COP, is considerably smaller because of the larger temperature span. Due to the relative increase in Joule heating the Carnot efficiency in test 2 has become smaller. The axial conduction in undesired direction cannot be a reason for lower COP in test 2 because the number of MCM layers have increased proportionally to the temperature span. A way to increase the efficiency while keeping the cooling capacity unchanged is lowering the current in Peltier elements but giving them more time to transfer heat. For example, in test 1 by reducing the current by the factor of 1.5 and activating Peltier elements 37.5% of the period instead of 25%, COP of 13.39 corresponding to Carnot efficiency of 4.5 is achieved with even slightly higher cooling capacity.

The lower COP in test 2 results in less heat absorbed at the cold end per cycle (heat rates in test 2 should be divided by ten to obtain heat per cycle), while the input energy to the system per cycle has not varied much. However, because of the higher frequency the cooling capacity in test 2 is larger than test 1. It should be noticed that in this design the electric current, similar to the flow rate of heat transfer fluid in conventional magnetic refrigeration cycle, should increase together with the frequency to get higher capacity; otherwise, the heat generated at higher rate during magnetization will not be taken from the MCM effectively.

As shown in Fig. 10, reducing the length of SC, although needed to reduce the thermal inertia of the system at higher frequencies, can result in low cooling capacity and COP as it lowers the thermal resistance of inactive PE against axial conduction. On the other hand, increasing the thermal resistance of PE by increasing its length is accompanied by escalated Joule heating reducing COP. Considering that PE may transfer heat from higher to lower temperature (from magnetized to demagnetized layer) when the number of layers are high enough, high thermal resistance can also have negative effect on transferring heat in the desirable direction.

With too low electric currents activating PE, both cooling capacity and COP are low since the Peltier elements cannot transfer enough heat from the magnetized MCM layers. When the cooling power is increased through increasing the cooling power of Peltier elements, the temperature at their cold end goes further down during their active period resulting in less efficient operation of Peltier elements at their increased temperature span. The gain in cooling power through increasing electric current eventually becomes negative as the quadratic growth of Joule heating captures the linear increase of Peltier effect. In multilayer arrays, the load on each PE is different with an increase from the cold end to the warm end of the array. Ideally, the geometry and electric current for each PE should be found separately for the best results, which complicates optimization further.

The number of parameters affecting the performance of hybrid Peltier element-magnetic cooling devices are high: Geometry of PE legs, copper, ceramic plates, and MCM layers; electric current exciting each PE; strength and pattern of variation of magnetic field; duration of each process;

cycle frequency; number of layers of MCM; Curie temperature of each layer; materials chosen as semiconductor, magnetocaloric materials, and ceramic. Apart from copper and ceramic parts, whose lower lengths are almost always desirable, all the parameters are tightly interconnected. Accordingly, optimization of such devices through parameter sweep requires simulating huge number of combinations of the parameters unless some parameters are grouped or some monotonic behaviors are identified.

The Peltier elements in the studied system are analogous to heat transfer fluid in conventional magnetic refrigeration systems in the sense that both the Peltier elements and the pumped heat transfer fluid carry net positive energy from the cold end to the warm end. In the test results summarized in Table 3, the power consumption of the Peltier elements is few times higher than the magnetic work, whereas, in a well-designed conventional magnetic refrigeration system with heat transfer fluid, the pumping power is usually smaller than the magnetic work. In a parametric study (not included in this article) in which I , L_{SC} , number of MCM layers, cycle period, and share of magnetization/demagnetization processes from the whole cycle period were varied about the values reported for test 1, no combination was found in which the relative power consumption of the Peltier elements are substantially reduced. Accordingly, use of Peltier elements as thermal diodes may not result in a highly efficient system unless Peltier modules with optimized geometry, optimized electric current and highly effective semi-conductor material, which show high efficiency at the small or even negative temperature span that the magnetized and demagnetized MCM layers create for them, are used.

Passive thermal diodes may seem interesting from efficiency point of view; however, it should be investigated in each case if they can conduct the heat in the desired direction fast enough considering the practical limitations in manufacturing and material properties.

5 Acknowledgement

The author would gratefully like to acknowledge that this study was financed by the Swedish Energy Agency, grant number 40330-1, and Electrolux through the research program EFFSYS EXPAND. I would also like to thank Prof. Björn Palm and Prof. Jesper Ooppelstrup for their suggestions and sharing time.

6 References

- Bartholomé, K., Hess, T., Mahlke, A., König, J., 2016. New concept for magnetocaloric heat pumps based on thermal diodes and latent heat transfer. 7th Int. Conf. Magn. Refrig. Room Temp., Thermag VII, Turin.
- Crank, J., 1975. The Mathematics of Diffusion, second ed. Clarendon Press, Oxford.
- Dhatt, G., Touzot, G., Lefrancois, E., 2012. Finite Element Method, John Wiley & Sons.
- Engelbrecht, K., 2008. A Numerical Model of an Active Magnetic Regenerator Refrigerator with Experimental Validation (Ph.D. dissertation). University of Wisconsin-Madison.
- Goldsmid, H. J., 1964. Thermoelectric Refrigeration, first ed., Springer.

- Hodes, M., 2005. On one-dimensional analysis of thermoelectric modules (TEMs). , IEEE Trans. Compon. Packag. Tech., 28 (2), 218-229. doi: 10.1109/TCAPT.2005.848532.
- Kitanovski, A., Tušek, J., Tomc, U., Plaznik, U., Ožbolt, M., Poredoš, A., 2015. Magnetocaloric Energy Conversion: From Theory to Applications, Springer.
- Li, H.B., Jiang, Q., Xu, X.N., Lu, D.W., 2016. A new concept refrigeration model based on thermal switch and numerical calculation. 7th Int. Conf. Magn. Refrig. Room Temp., Thermag VII, Turin.
- Lozano, J. A., Engelbrecht, K., Bahl, C. R. H., Nielsen, K. K., Barbosa Jr, J. R. , Prata, A. T. , Pryds., N., 2014. Experimental and numerical results of a high frequency rotating active magnetic refrigerator. Int. J. Refrigeration 37, 92-98. doi: <http://dx.doi.org/10.1016/j.ijrefrig.2013.09.002>.
- Monfared, B., 2016. Simulation of magnetic refrigeration systems with thermal diodes and axial conductive heat transfer. 7th Int. Conf. Magn. Refrig. Room Temp., Thermag VII, Turin.
- Monfared, B., Palm, B., 2015. Optimization of layered regenerator of a magnetic refrigeration device. Int. J. Refrigeration 57, 103-111. doi: <http://dx.doi.org/10.1016/j.ijrefrig.2015.04.019>.
- Olsen, U. L., Bahl, C. R. H. , Engelbrecht, K., Nielsen, K. K., Tasaki, Y., Takahashi, H., 2014. Modeling of in-vehicle magnetic refrigeration. Int. J. Refrigeration 37, 194-200. doi: <http://dx.doi.org/10.1016/j.ijrefrig.2013.09.013>.
- Qian, S., Nasuta, D., Rhoads, A., Wang, Y., Geng, Y., Hwang, Y., Radermacher, R., Takeuchi, I., 2016. Not-in-kind cooling technologies: A quantitative comparison of refrigerants and system performance. Int. J. Refrigeration, 62, 177-192. doi: <http://dx.doi.org/10.1016/j.ijrefrig.2015.10.019>.
- Silva, D. J., Ventura, J., Araújo, J. P., Pereira, A. M., 2014. Maximizing the temperature span of a solid state active magnetic regenerative refrigerator. Appl. Energy 113, 1149-1154. doi: <http://dx.doi.org/10.1016/j.apenergy.2013.08.070>.
- Tasaki, Y., Takahashi, H., Yasuda, Y., Okamura, T., Ito, K., 2012. A study on the fundamental heat transport potential of an in-vehicle magnetic refrigerator. 5th Int. Conf. Magn. Refrig. Room Temp ., Grenoble.
- Tomc, U., Tušek, J., Kitanovski, A., Poredoš, A., 2013. A new magnetocaloric refrigeration principle with solid-state thermoelectric thermal diodes. Appl. Thermal Eng. 58 (1–2):1-10. doi: <http://dx.doi.org/10.1016/j.applthermaleng.2013.03.063>.
- Tomc, U., Tušek, J., Kitanovski, A., Poredoš, A., 2014. A numerical comparison of a parallel-plate AMR and a magnetocaloric device with embodied micro thermoelectric thermal diodes. Int. J. Refrigeration, 37, 185-193. doi: <http://dx.doi.org/10.1016/j.ijrefrig.2013.07.003>.

Supplementary content

This video shows temperature, magnetic field, and electric current changes during a cycle after reaching steady state for test 2, described in section 3.



Video Supplementary material.mp4

Video 1 one cycle after test 2 reaches steady state

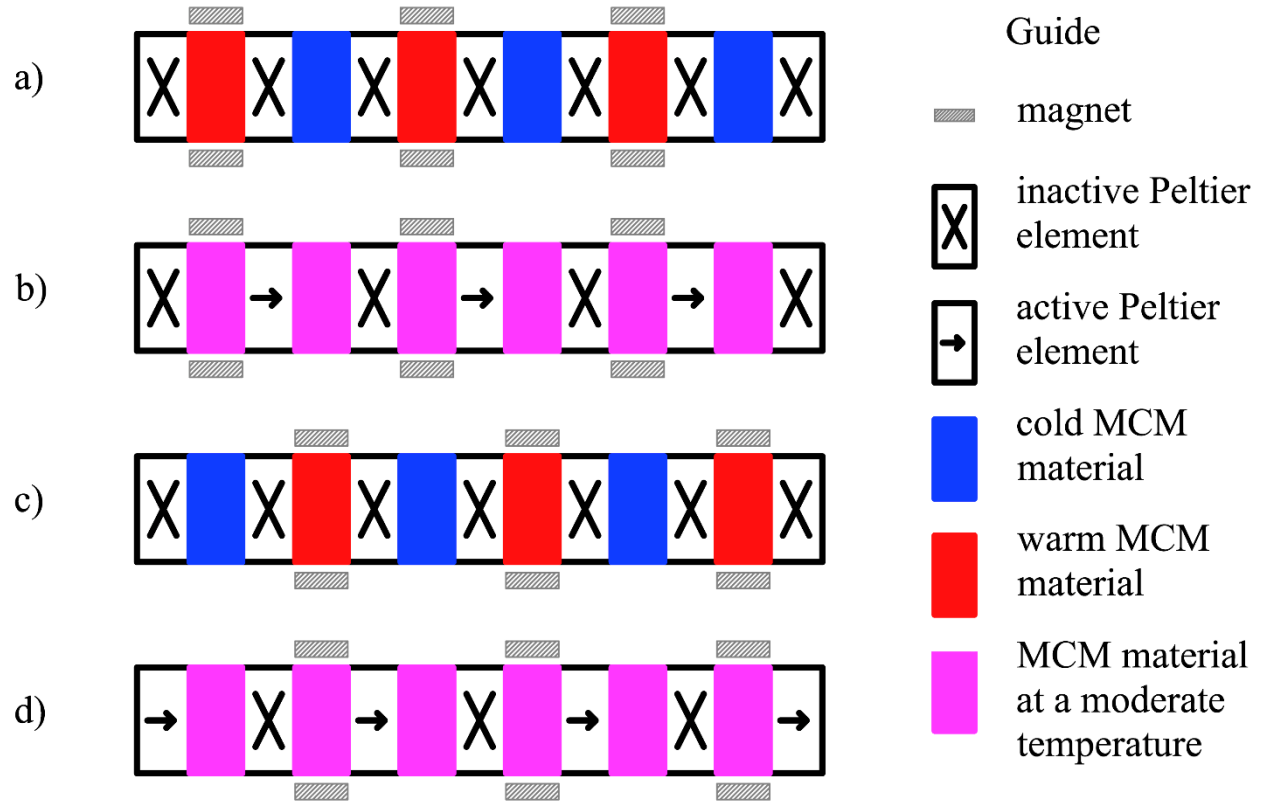


Fig. 1 working principle of the modeled solid-state magnetic refrigeration device

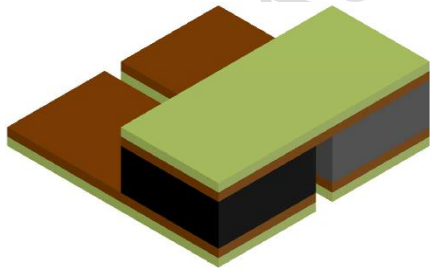


Fig. 2 schematic drawing of a single Peltier element. Grey and black colors show the semiconductor legs. The copper and ceramic layers are shown by brown and green.

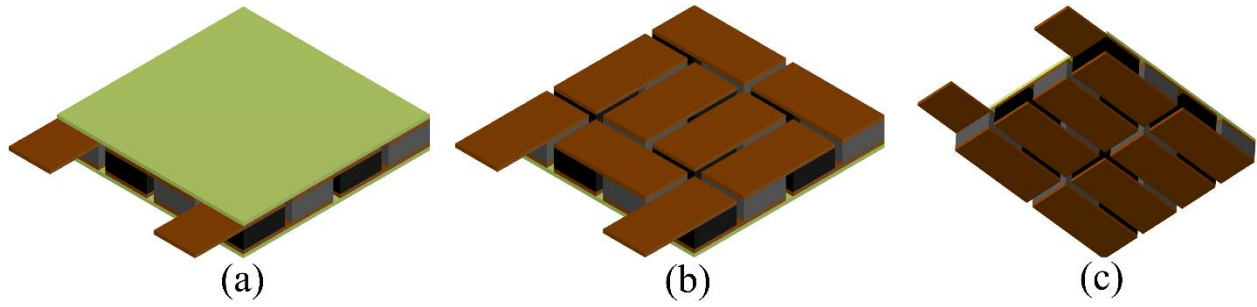


Fig. 3 a thermoelectric module which consists of 8 Peltier elements (16 legs). In (b) and (c) the upper and lower ceramic layers are removed to show the electric connection of the elements



Fig. 4 sequence of placement of the materials (for a case with 3 layers of MCM)

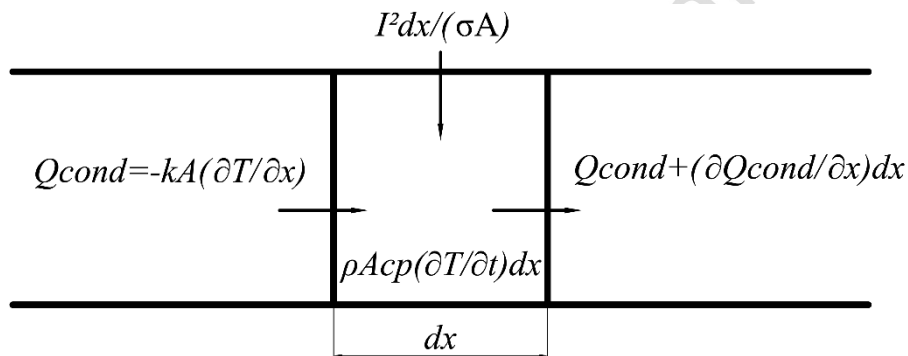


Fig. 5 energy balance over infinitesimal element of PE (Peltier effect term is not shown)

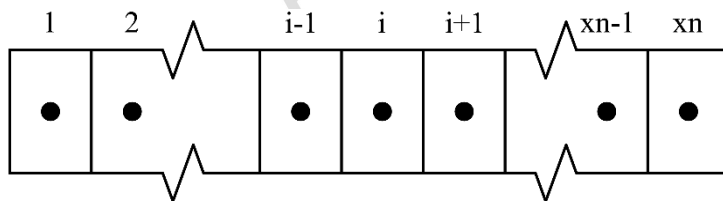


Fig. 6 cells and temperature nodes in FVM

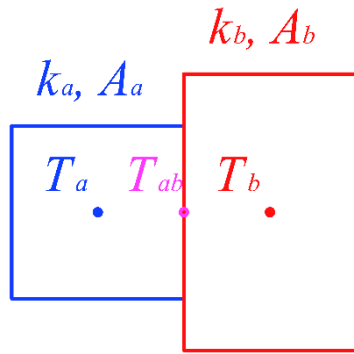


Fig. 7 varying cross section area and conductivity between temperature nodes in the finite volume model

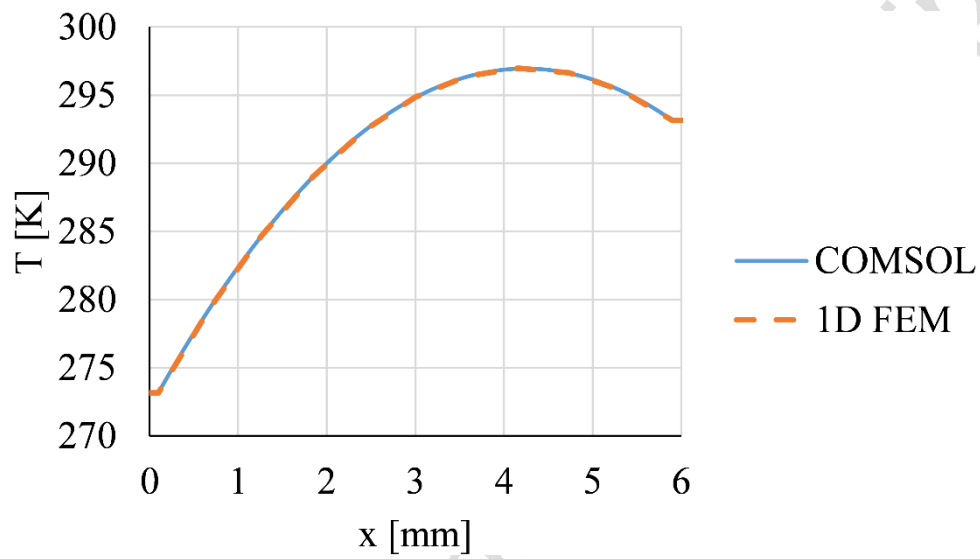


Fig. 8 comparing the temperatures calculated by the developed 1D FEM model and by COMSOL

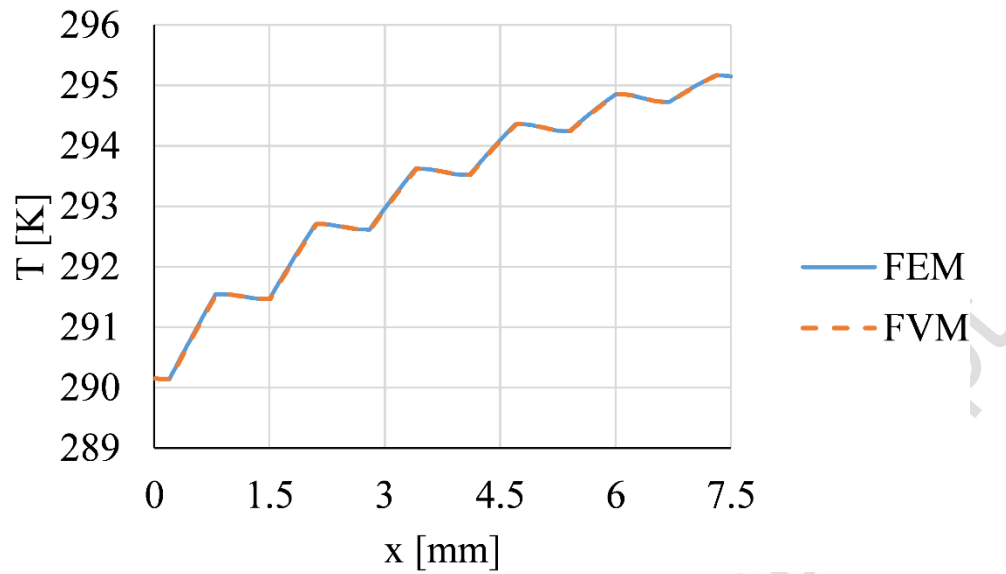


Fig. 9 comparing the average cycle temperatures calculated by finite element and finite volume models for test 2

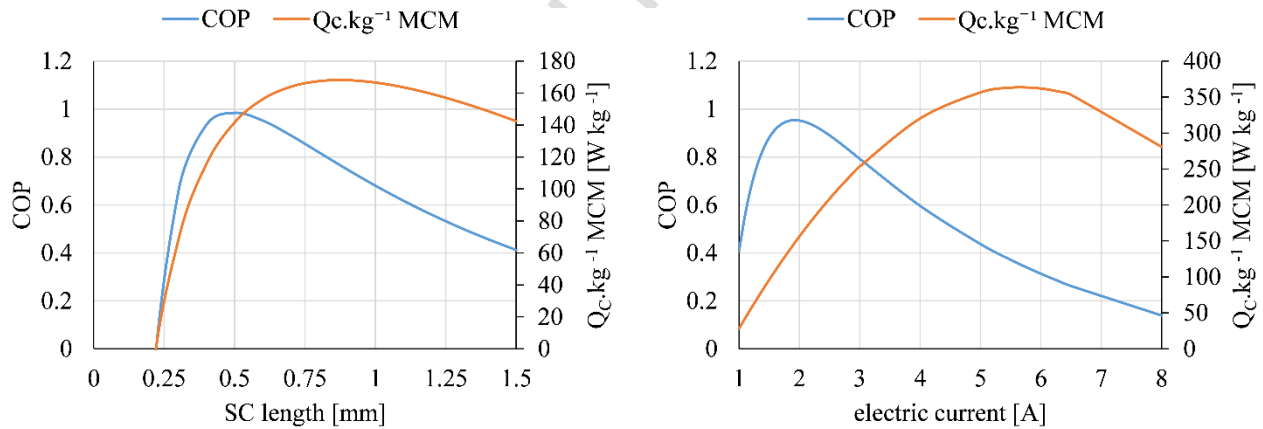


Fig. 10 varying the length of the semiconductor and the electric current with the rest of the parameters of test 2 unchanged

Table 1 comparing our model of Peltier element with COMSOL results

	COMSOL	FEM	error [%]
Q_C [W]	0.03365	0.03363	-0.06
Q_H [W]	0.05669	0.05666	-0.05
El_{PE} [W]	0.02304	0.02303	-0.04
COP	1.4607	1.4604	-0.02

Accepted Manuscript

Table 2 common input values used for FEM against FVM validation tests

input parameter	test 1	test 2	unit
Δx	0.025	0.025	mm
L_{SC}	0.6	0.6	mm
L_{MCM}	0.3	0.3	mm
L_C	0.1	0.1	mm
L_{Cu}	0.1	0.1	mm
I	1	2	A
B_{max}	1	1	T
T_{HE}	295.15	295.15	K
T_{CE}	294.15	290.15	K
A_{SC}	5.76	5.76	mm ²
A_{MCM}	7.29	7.29	mm ²
A_C	7.29	7.29	mm ²
A_{Cu}	6.24	6.24	mm ²
τ_1, τ_2, τ_3 and τ_4	0.25	0.025	s
semiconductor	Bi-Te	Bi-Te	
ceramic	alumina	alumina	
layers of MCM	1	5	

Table 3 comparing finite element and finite volume models. For test 1 and test 2 average of FEM and FVM results are given.

	test 1	test 2	test 1	test 2	error	error
	0.017 g MCM	0.086 g MCM	per kg MCM	per kg MCM	test 1	test 2
					[%]	[%]
Q_C [W]	0.0090	0.0135	523	156	0.3	0.0
Q_H [W]	0.0100	0.0276	580	319	0.2	0.4
El_{PE} [W]	0.0009	0.0105	51.5	122	0.9	0.0
W_{mag} [W]	0.0001	0.0035	5.38	41.0	0.9	3.3
COP	9.21	0.96	9.21	0.96	1.1	0.8
η_C [%]	3.1	1.7	3.1	1.7	1.1	0.8